J. Fluid Mech. (1983), *vol.* 133, *pp.* 265–285
Printed in Great Britain

On the force fluctuations acting on a circular cylinder in crossflow from subcritical up to transcritical Reynolds numbers

By GÜNTER SCHEWE
DFVLR-Institut für Aeroelastik (AVA), D-3400 Göttingen, Germany

(Received 23 November 1982 and in revised form 12 April 1983)

Force measurements were conducted in a pressurized wind tunnel from subcritical up to transcritical Reynolds numbers $2.3 \times 10^4 \leqslant Re \leqslant 7.1 \times 10^6$ without changing the experimental arrangement. The steady and unsteady forces were measured by means of a piezobalance, which features a high natural frequency, low interferences and a large dynamic range. In the critical Reynolds-number range, two discontinuous transitions were observed, which can be interpreted as bifurcations at two critical Reynolds numbers. In both cases, these transitions are accompanied by critical fluctuations, symmetry breaking (the occurrence of a steady lift) and hysteresis. In addition, both transitions were coupled with a drop of the C_D value and a jump of the Strouhal number. Similar phenomena were observed in the upper transitional region between the super- and the transcritical Reynolds-number ranges. The transcritical range begins at about $Re \approx 5 \times 10^6$, where a narrow-band spectrum is formed with $Sr(Re = 7.1 \times 10^6) = 0.29$.

1. Introduction

The flow around a circular cylinder is a classical problem of fluid dynamics, knowledge of which is essential for basic understanding as well as for technical applications. Flow-induced forces which are coupled with formation of the vortex street behind the cylinder, particularly in the case of very high Reynolds numbers, are important in technical applications. Because it is difficult to achieve very high Reynolds numbers in a wind-tunnel experiment, there are only a few investigations for $Re \gtrsim 5 \times 10^6$ in incompressible flow. Interest was drawn to the very high Reynolds-number range by Roshko (1961), who detected the reappearance of definite vortex shedding in this range, which he called transcritical. Up to that time it was believed that, after the boundary-layer transition in the critical range, the regular vortex shedding would cease and that, for a Reynolds number approaching infinity, the flow past a circular cylinder would approach chaotic state. The following investigations performed by Achenbach (1968), Jones, Chincotta & Walker (1969) and James, Paris & Malcolm (1980) confirmed Roshko's findings and thus extended our knowledge of the transcritical range, but the cylinders used were too large or the velocities too high. As a consequence of blockage or compressibility effects, the scatter of the measured quantities was rather high. In addition, the essential question concerning the physical reasons for the reappearance of an ordered flow pattern at very high Reynolds numbers remains open.

Apart from the transcritical range, the observed phenomena and the experimental results down to subcritical Reynolds number $Re \approx 10^5$ are quite different. One reason

for this is that, especially at critical and supercritical Reynolds numbers, sensitivity of the flow to even the smallest perturbations, caused for example by test conditions, is very high. The second reason is the fact that, besides the Reynolds number, the stability of the flow is influenced by additional parameters such as turbulence intensity of the wind tunnel, Mach number and surface roughness.

In the critical range, asymmetric flow separation coupled with steady lift was observed (Kraemer 1964; Bearman 1969; Kamiya, Suzuki & Nishi 1979), which is probably caused by a one-sided laminar separation bubble (Bearman). The measured lift force had consistently the same sign (Kraemer; Bearman) or always the same sign for increasing and the opposite for decreasing Reynolds number (Kamiya *et al.*). These findings suggest the question whether such phenomena are fundamental or caused by asymmetric test conditions. The present study will demonstrate that the phenomenon is fundamental, because it was found that the occurrence of both signs for the steady lift is possible. Beyond a critical Reynolds number the symmetric flow pattern becomes unstable against an asymmetric flow pattern. This transition from a symmetric to an asymmetric flow state can be interpreted as a subcritical bifurcation. The abrupt disappearance of the asymmetric flow state can be explained in a similar manner.

The present force measurements were conducted in a new wind tunnel in Göttingen, which can be pressurized up to 100 bar; thus the obtainable Reynolds number is very high. Measurements were taken from subcritical up to transcritical Reynolds numbers without changing the cylinder (blockage 10 %) or any other component of the experimental arrangement. Owing to the large range and the high ambient pressure, development of a new force balance able to cope with the extreme demands in the high-pressure wind tunnel was necessary. This new balance based on piezoelectric–multicomponent force elements features a high natural frequency, a large dynamic range and low interferences. Using the high-pressure wind tunnel in conjunction with the piezobalance, it is possible to overlap the individual Reynolds number ranges by merely varying the flow parameters.

2. Experimental arrangement

2.1. *The high-pressure wind tunnel*

The high-pressure wind tunnel is described in detail by Försching, Melzer & Schewe (1981). The entire wind tunnel, which is of closed-return type, can be pressurized up to 100 bar and its closed square test section measures 0.6×0.6 m. The test section (length 1 m) has four slots (width 0.01 m), one in each corner. With a maximum flow velocity of about $u_\infty = 38$ m/s and maximum pressure of $p = 100$ bar, a Reynolds number of $Re = 1.2 \times 10^7$ may be reached. The maximum diameter of the circular cylinder in this case is 0.06 m, yielding a geometric blockage of 10 %. The minimum Reynolds number is about $Re = 10^4$ at atmospheric pressure and $u_\infty \approx 3$ m/s. Thus a variation of three orders of magnitude for the Reynolds number is possible. The turbulence intensity of the free stream increases slightly with the Reynolds number and is less than 0.4 %. For all measurements the same circular cylinder was used with a diameter $D = 0.06$ m and a length $L = 0.6$ m (aspect ratio $L/D = 10$). The surface of the cylinder was painstakingly finished and finally polished.

2.2. *The piezobalance*

The difficulty of measuring unsteady forces is attributable to the fact that the balance/model system is basically an accelerometer whose resonance frequencies lie in the frequency range of interest, especially in the case of strain-gauge balances.

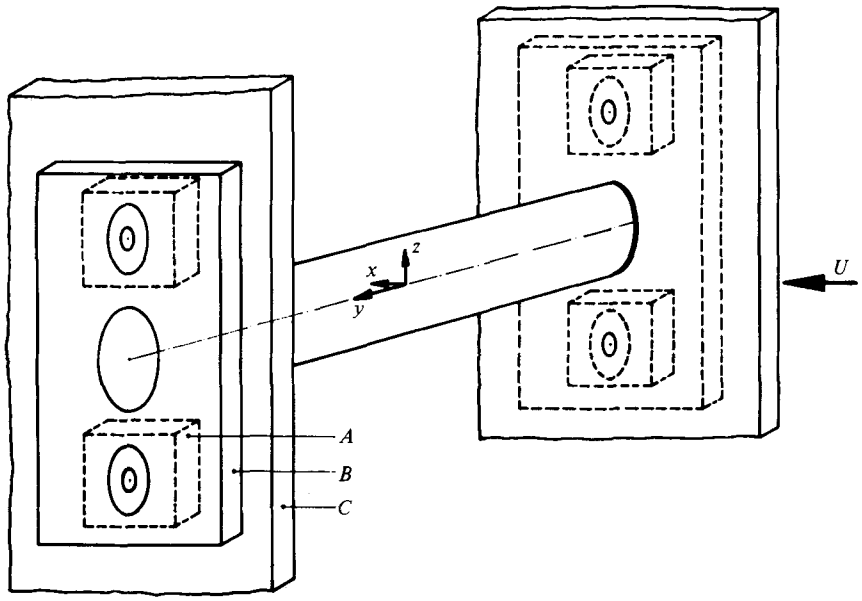

FIGURE 1. Schematic drawing of the arrangement of the balance: (*A*) 3-component load washer; (*B*) force-conducting top plate; (*C*) wall of the test-section, *U*-flow direction.

Therefore the new balance is based on 3-component piezoelectric force-measuring elements (Kistler Instrumente, Type 9067), which were modified by the manufacturer for use up to 100 bar. As illustrated by figure 1, the balance is constructed of four load washers. With the aid of elastic bolts and a common top plate (*B*), two load washers are pressed to each vertical wall (*C*) of the test section, so that the shear forces on the load washers can be transmitted by friction. The freely suspended test cylinder is then passed through the wall and clamped on both sides onto the force-conducting top plate (*B*). There is a small gap (0.5 mm) between the surface of the cylinder and the hole in the wall of the test section. Thus a slight flow leakage is unavoidable.

Using a charge amplifier (Kistler Type 9007) the effective measuring time for quasistatic measurements is limited by the exponential decay of the charge with time constants of 10^3–10^6 s (depending on measuring range), and leakage currents in the charge amplifier. Both effects cause the zero point to drift. If for example the time $T_{1\,\%}$ (referring to an error of 1 %) is defined, then a value of $T_{1\,\%} = 17$ min was obtained for a static load of $F = 25$ N. Quasistatic measurements are possible down to about 5 N and with reduced accuracy to 1 N. The maximum load can be 10 kN where the threshold for dynamic measurements is as low as 0.01 N. Interference between the drag F_x and the lift F_z and vice versa is lower than 1 %. Because of the high rigidity of the quartz elements themselves, the natural frequency of the balance is determined by the cylinder which connects both parts of the balance. The lowest eigenfrequency was $f = 385$ Hz for the F_x component, where $f = 180$ Hz was the highest measured vortex-shedding frequency in the present experiments. For more details concerning the balance see Schewe (1982).

Evaluation of the signals was performed by means of a Nicolet 660 B FFT analyser and a digital computer equipped with an analog-to-digital converter.

3. Experimental results

The measurements were taken from sub- up to transcritical Reynolds numbers $2.3 \times 10^4 \leqslant Re \leqslant 7.1 \times 10^6$ without changing the experimental setup. The flow parameters were varied as follows: 1 bar $\leqslant p \leqslant$ 51 bar and 4 m/s $\leqslant u_\infty \leqslant$ 38 m/s. The present experiments were not extended up to 100 bar because of difficulties with the corrugated hoses in which the measuring cables are led out of the wind tunnel. The nomenclature for the different Reynolds-number ranges is that proposed by Roshko (1961). None of the results presented here have been corrected for wind-tunnel blockage effects. The likely extent of corrections will be discussed in §3.1.1.

3.1. *Reynolds-number range from* 2×10^4 *up to* 7×10^6

3.1.1. *The drag coefficient*

In figure 2(*c*) the C_D values are plotted against Re. The results match the classical measurements (Wieselsberger 1923) except for the somewhat steeper decrease of the curve for $Re < 5 \times 10^4$. We will refer to this point in §3.1.4. In the critical range there are two discontinuous drops of C_D (A and B) in the supercritical state, which begins at $Re = 3.5 \times 10^5$. The C_D value is nearly constant up to about $Re \approx 10^6$ with $C_D = 0.22$. The remarkable feature of this supercritical range is its extent up to $Re \approx 10^6$, which is probably an indication for good test conditions. Behind a second transitional range ($10^6 \lesssim Re \lesssim 5 \times 10^6$), in which C_D is increasing again, there is a further plateau where C_D is nearly constant with $C_D = 0.52$ (transcritical range; $Re \gtrsim 5 \times 10^6$). The agreement with Jones *et al.* (1969) is good. In comparison with other known results in the transcritical range, there seems to be no significant correlation between the aspect ratio L/D and the measured drag coefficients. Although Roshko (1961) and Jones *et al.* (1969) used the same aspect ratio ($L/D = 5$), they measured $C_D = 0.7$ and $C_D = 0.5$ respectively. The higher C_D value measured by Roshko (1961) and Achenbach & Heinecke (1981) are probably caused by higher surface roughness, as was found by Roshko (1970).

Finally, we make an estimate as to the likely extent of wind-tunnel blockage effects. The method of Allen and Vincenti (see e.g. Roshko 1961) was applied to the present measurements. The measured values are denoted by an asterisk (u^* and C_D^*). In the subcritical state the required correction for the velocity and drag coefficients would be $u/u^* = 1.04$ and $C_D/C_D^* = 0.92$; in the supercritical state $u/u^* = 1.01$ and $C_D/C_D^* = 0.96$, and in the transcritical state $u/u^* = 1.02$ and $C_D/C_D^* = 0.95$. The above corrections are slightly too high since the method is valid for a closed test section, whereas our wind tunnel has four small slots. None of the results presented here, however, have been corrected for the reason that there is no method valid for such a large Reynolds-number range in which the separation point moves. Further, we know of no method for correcting fluctuating force measurements.

3.1.2. *Measurement of Strouhal numbers*

In Figure 2(*b*) the Strouhal numbers $Sr = fD/u_\infty$ are plotted against Re with f as the frequency of the lift fluctuations. They were obtained from the power spectra $\Phi_L(f)$ of the lift fluctuations. In the case of a single narrow peak in the power spectrum, the Strouhal number is identical with the vortex-shedding frequency. This is valid outside the transitional regimes. The meaning of the Strouhal number in the critical regime and the upper transition should become clearer in the discussion of the appropriate power spectra. In the subcritical range the Strouhal number amounts to $Sr = 0.2$ and the scatter of the measured values is very low. The critical range

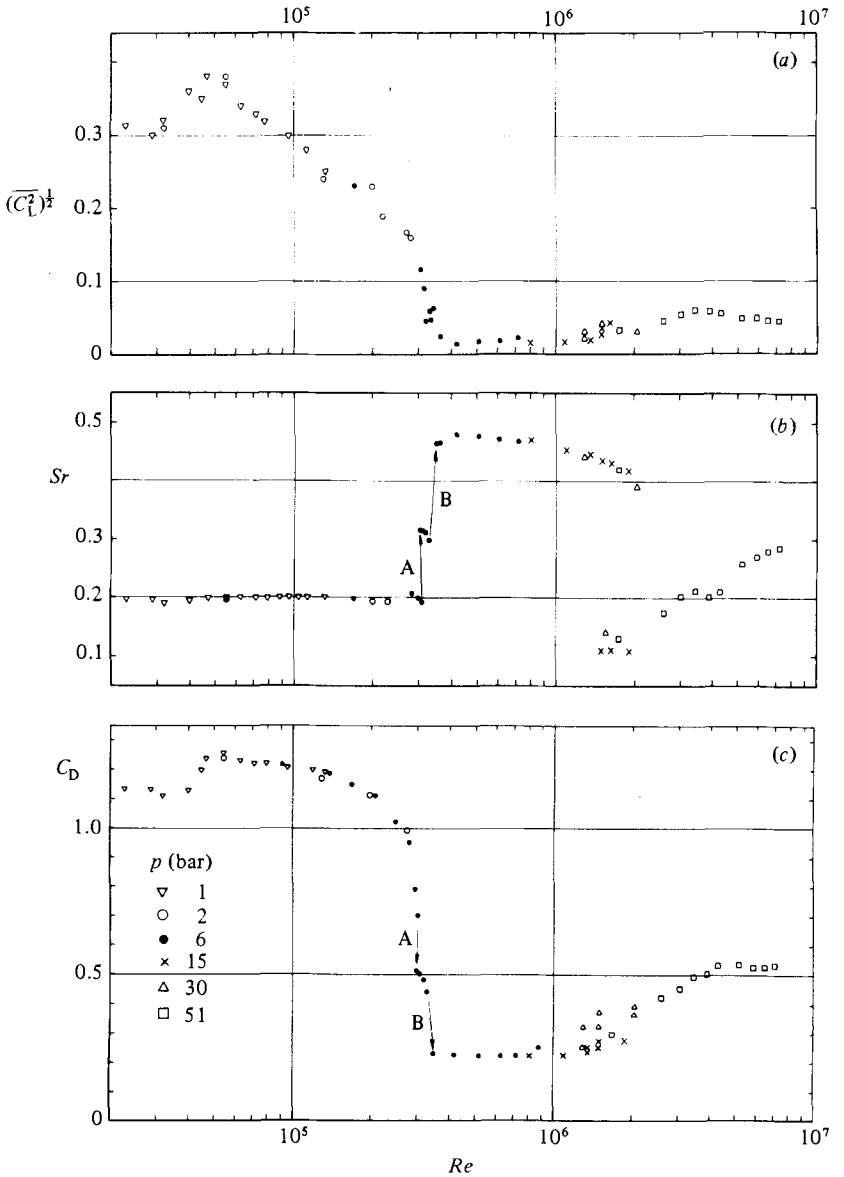

FIGURE 2. (*a*) R.m.s. of the lift fluctuations. (*b*) Strouhal number of the lift fluctuations, $Sr = fD/u_\infty$. (*c*) Drag coefficient.

exhibits two discontinuous transitions A and B, where the Strouhal number jumps to 0.3 and then to 0.48, which confirms the measured values of Bearman (1969) and Achenbach & Heinecke (1981). These two jumps are directly coupled with the two drops of the C_D coefficient (figure 2*c*). In a later section these transition phenomena will be described and discussed in detail. At supercritical Reynolds numbers the Strouhal number remains nearly constant as long as the drag coefficient is minimal. The following upper transition exhibits a slightly decreasing Strouhal number down to about $Sr \approx 0.4$ at $Re \approx 2 \times 10^6$. Finally for the highest Reynolds number reached in the present investigation ($Re = 7.1 \times 10^6$) a value of $Sr = 0.29$ was determined, which is in good agreement with Jones *et al.* (1969). Roshko (1961) found $Sr = 0.27$, which is approximately the same result, considering the different flow configurations.

Achenbach & Heinecke (1981) obtained $Sr \approx 0.25$ at $Re = 4 \times 10^6$, where the transcritical range is just beginning. The Strouhal numbers measured by James *et al.* (1980) are lower than the present ones and exhibit a large scatter with $Sr = 0.22 \pm 0.02$.

3.1.3. *Power spectra of the lift fluctuations*

Figure 3 illustrates six power spectra $\Phi_L(f)$ of the lift fluctuations, which belong to the individual Reynolds-number ranges. The five spectra (figures 3*a–e*) demonstrate the unique option offered by a wind tunnel with variable density. The Reynolds number was changed only by varying the properties of the fluid, while the flow velocity and the geometrical parameters remained nearly constant (1 bar $\leqslant p \leqslant$ 51 bar; $u_\infty = 32 \pm 0.5$ m/s). The spectrum (figure 3*f*) was taken at the highest Reynolds number reached, $Re = 7.1 \times 10^6$ ($u_\infty = 38$ m/s; $p = 51$ bar). The abscissa has a Strouhal-number scale and the ordinate was dimensionalized such that the integral of the spectrum results in the mean square of the lift coefficient $\overline{C_L^2}$:

$$\overline{C_L^2} = \int \Phi_L(f) \frac{u_\infty}{q_\infty^2 A^2 D} d\left(\frac{fD}{u_\infty}\right),$$

where q_∞ is the dynamic pressure and A the area of the cylinder.

Because of this normalization, all spectra are comparable with respect to their characteristic shape, effective width of the peaks or other features. No corrections or other manipulations have been applied to the spectra. Disturbances (dotted lines) which are evident in figures 3(*b–d*) are probably caused by vibrations of the entire wind tunnel. Figure 3 (*a*) shows a narrowband spectrum ($Sr = 0.2$) taken at subcritical Reynolds number $Re = 1.3 \times 10^5$. The second spectrum (figure 3*b*) is characteristic for supercritical Reynolds numbers with a remarkably narrow peak even at $Re = 7 \times 10^5$. The state of the flow seems to be very stable, as indicated by the absence of low-frequency fluctuations. The Strouhal number nearly has its maximal value $Sr = 0.47$, which is probably related to the previous findings that C_D is constant (minimal) up to $Re \approx 10^6$.

In the upper transitional range $10^6 \lesssim Re \lesssim 5 \times 10^6$ there is no typical spectrum. The example presented here (figure 3*c*) recorded at $Re = 1.9 \times 10^6$ has two broad maxima. The centroid of the area of the low-frequency part is located at about $Sr \approx 0.1$. The small broad maximum at $Sr \approx 0.42$ probably corresponds to the supercritical flow state and has nearly disappeared. In this case for example, where the peaks in the spectrum are not sharp, the Strouhal number cannot be considered a vortex-shedding frequency. The measured spectra in this upper transition are dissimilar with respect to their characteristic shape. Apart from this spectrum there are spectra with monotonically decreasing $\Phi_L(f)$ from low up to higher frequencies without any marked feature. Another type of spectrum was characterized by a pronounced maximum at $Sr \approx 0.1$ and monotonically decreasing $\Phi_L(f)$ for increasing f. In the range $10^6 \lesssim Re \lesssim 2 \times 10^6$ steady lift forces up to $|C_L|/C_D \approx 0.4$ (both signs possible) were observed, which were often coupled with a broad maximum in the power spectrum at about $Sr \approx 0.1$. So far no definite correlations between an occurrence of lift (asymmetric flow state), the C_D value and the feature of the power spectrum could be found.

The power spectra in figures 3(*e, f*) are typical for very high Reynolds numbers $Re \gtrsim 5 \times 10^6$. The development to the narrow peak (figure 3*f*) is as follows. Beginning at about $Re \approx 2.5 \times 10^6$, a reproducible broad maximum is formed (figure 3*d*) whose Strouhal number increases slightly with increasing Reynolds number (figure 2*b*). The presence of low-frequency fluctuations with high intensity indicates that the end of

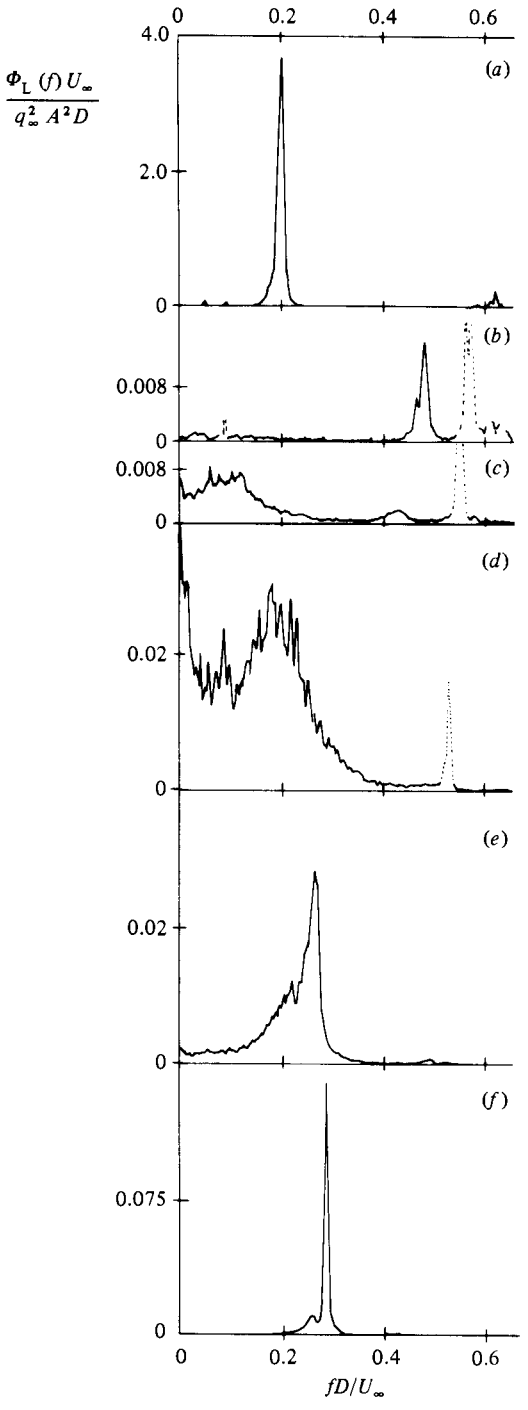

FIGURE 3. Power spectra of the lift fluctuations ($A = LD$). (*a*) Subcritical; $Re = 1.3 \times 10^5$, $p =$ 1 bar, $u_\infty = 32$ m/s. (*b*) Supercritical; $Re = 7.2 \times 10^5$, $p = 6$ bar, $u_\infty = 32$ m/s. (*c*) Transition super- to transcritical; $Re = 1.9 \times 10^6$; $p = 15$ *bar*, $u_\infty = 32$ m/s. (*d*) Near the end of the upper transition; $Re = 3.7 \times 10^6$, $p = 30$ bar, $u_\infty = 32$ m/s. (*e*) Beginning of the transcritical range; $Re = 5.9 \times 10^6$, $p = 51$ bar, $u_\infty = 32$ m/s. (*f*) Transcritical; $Re = 7.1 \times 10^6$, $p = 51$ bar, $u_\infty = 38$ m/s.

the transitional regime is not yet reached. Beginning with about $Re \approx 5.5 \times 10^6$ a new peak at about $Sr \approx 0.27$ is continuously growing (figures 3*e*, *f*). With increasing Reynolds number the new peak becomes higher and narrower with a corresponding slight increase of the Strouhal number (figure 2*b*) and the broad maximum becomes smaller down to the residual peak at $Sr = 0.26$ (figure 3*f*). Finally the small jump of Sr at $Re \approx 5 \times 10^6$ results from the fact that the power spectrum for $2.5 \times 10^6 \lesssim Re \lesssim 7 \times 10^6$ exhibits two parts. For $Re < 5 \times 10^6$ the broadband maximum dominates at $Sr \approx 0.2$, where the range $Re > 5 \times 10^6$ is dominated by the newly developed narrow peak with $Sr \gtrsim 0.27$.

3.1.4. *R.m.s. values of the lift fluctuations*

For the sake of comparison the r.m.s. values of the lift fluctuations $(\overline{C_L^2})^{\frac{1}{2}}(Re)$ are plotted in figure 2(*a*) together with $C_D(Re)$ and $Sr(Re)$. The qualitative dependence of $(\overline{C_L^2})^{\frac{1}{2}}(Re)$ is according to the curve $C_D(Re)$. This curve has a maximum value of $(\overline{C_L^2})^{\frac{1}{2}} = 0.38$ in the subcritical regime ($Re \approx 5 \times 10^4$), where $C_D(Re)$ shows a sudden increase. In this context it is interesting to note that the base pressure coefficient $C_{p_{180}}$ is minimal at approximately the same Reynolds number with $C_{p_{180}}(Re \approx 5 \times 10^4) = -1.2$ (Roshko 1970). The minimal r.m.s. value amounts to 0.02 in the supercritical regime. At $Re \approx 3.5 \times 10^6$, where the broad maximum is formed in the spectrum (figure 3*d*), the r.m.s. value exhibits a slightly pronounced relative maximum. As Re is increased further, the development to the narrow peak (transcritical) is coupled with a slightly decreasing r.m.s. value and an increasing Strouhal number.

When interpreting these measurements, one has to bear in mind that the present total force measurements integrate in spanwise direction over possible variations of sectional forces. Most of the investigations performed at very high Reynolds numbers obtained the forces by integrating a sectional pressure distribution.

3.1.5. *Probability density distributions and its moments*

In figures 4 and 5 two typical probability density distributions $P(C'_L)$ are presented characteristic for the sub- and transcritical Reynolds-number ranges. The curves are normalized such that

$$\int P(C'_L)\,\mathrm{d}C'_L = 1.$$

For the sake of comparison the Gaussian probability distribution is included, because the deviation from the Gaussian distribution provides information about the nature of a process. The non-Gaussian effects are evident for example under close inspection of the tails of the measured probability density (figure 4). The probability that the amplitudes exceed the threshold $C'_L \approx \pm 2.8$ is considerably smaller than is the case for a Gaussian process.

The higher statistical moments skewness factor Sk and flatness factor Fl,

$$Sk = \frac{\overline{C_L^3}}{(\overline{C_L^2})^{\frac{3}{2}}}, \quad Fl = \frac{\overline{C_L^4}}{\overline{C_L^2}^2},$$

which characterize $P(C'_L)$ as well as the peak values of $C'_L(t)$, are calculated and recorded in table 1. The values of Sk and Fl, which are valid for example for a sine wave and a Gaussian process, are also included in table 1. An interpretation of these results will be given in the following discussion.

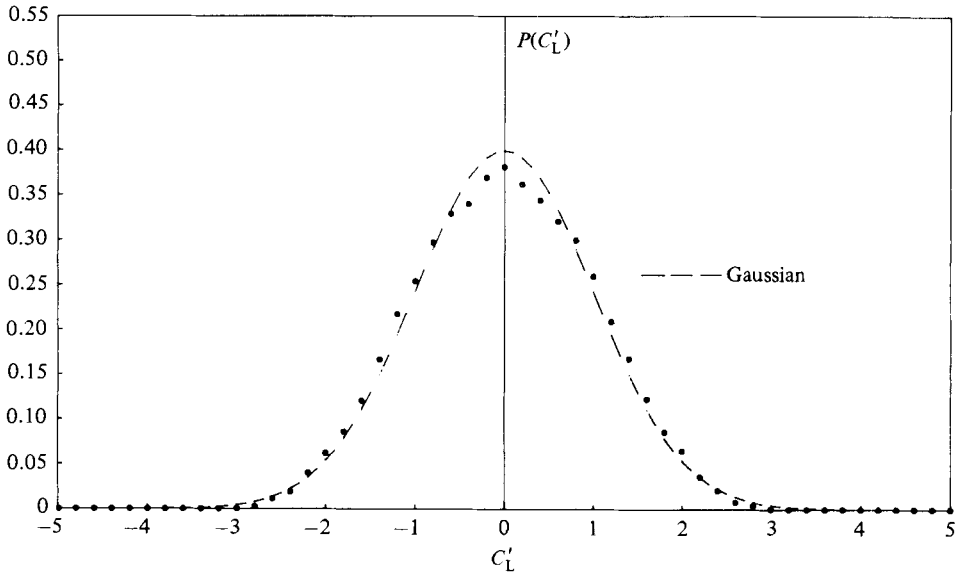

FIGURE 4. Probability density distribution of the lift fluctuations ($Re = 5.5 \times 10^4$, subcritical).

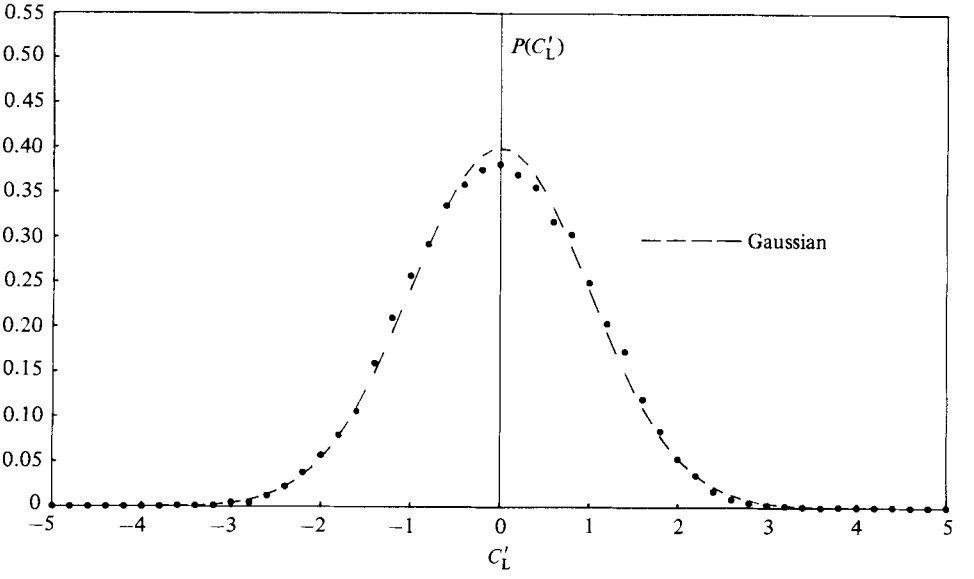

FIGURE 5. Probability density distribution of the lift fluctuations ($Re = 7.1 \times 10^6$, transcritical).

3.2. *The fine structure in the critical Reynolds number regime*

In the critical Reynolds-number regime the boundary-layer transition from laminar to turbulent flow is accompanied by a sudden increase of the Strouhal number (see e.g. Drescher 1956; Bearman 1969) and the occurrence of asymmetric flow states (Kraemer 1964; Bearman 1969; Achenbach & Heinecke 1981). By small increments of the wind-tunnel speed the fine structure of the critical Reynolds-number range was investigated. In figures 6 (c', b' and a') the drag $F_x(Re)$, the Strouhal number $Sr(Re)$ and the lift coefficient $C_L(Re)$ are plotted against Reynolds number (p = const). The

State	Re	Sk	Fl	C'_{Lpeak} (r.m.s.)
Subcritical	5.5×10^4	0.00	2.6	±3
Supercritical	3.5×10^5	0.01	2.8	$\begin{cases}+3.8\\-4.0\end{cases}$
Upper transition	2.6×10^6	−0.08	3.3	$\begin{cases}-4.0\\+4.4\end{cases}$
Transcritical	7.1×10^6	−0.02	2.8	$\begin{cases}-4.0\\+3.8\end{cases}$
Gaussian	—	0	3.0	—
Sine	—	0	1.5	$\pm\sqrt{2}$

TABLE 1. Statistical moments skewness factor Sk, flatness factor Fl and peak values C'_{L} for the individual Reynolds-number ranges

unusual representation of figure 6(c') (without any normalization) emphasizes the extreme of $F_x(Re)$ and the fine structure of the critical range. Evident is the relative minimum $F_x(Re = 3.5\times10^5)$, which is a sharp boundary between the critical and the supercritical ranges. The maximum at $F_x(Re) = 2.8\times10^5$ marks the end of the range where quasiperiodic lift fluctuations occur; the typical spectrum is characterized by a single narrow peak (figure 3a). This maximum also marks the onset of wideband low-frequency fluctuations and an increase of the width of the peak in the spectrum $\Phi_{\mathrm{L}}(f)$, while Re is increasing.

As mentioned in §3.1.1 (see figure 2), two discontinuous transitions A and B were observed. After transition A, a bistable asymmetric flow state occurred, accompanied by a drop of F_x, a steady lift $|C_{\mathrm{L}}| \approx 1$ (figure 6a') and a jump of the Strouhal number to $Sr = 0.3$ (figure 6b'). This state is called bistable because there are two stable states corresponding to both possible signs of the lift force. This flow state with $|C_{\mathrm{L}}|/C_{\mathrm{D}} \approx 2$ is stable for a small Reynolds-number range until the second transition B occurs. Transition B is characterized by a second drop of the drag F_x to almost its half, a further jump of the Strouhal number to $Sr = 0.48$ and the abrupt disappearance of the steady lift C_{L}.

In figure 6 the individual stages of the flow in the critical regime are denoted by lower-case letters (a–f). The related power spectra for these individual stages are pictured in figures 7(a–f). Both axes of the spectra are linear and no normalization was applied, so that the areas under the curves are proportional to the mean square of the lift fluctuations $\overline{F_z'^2}$ (the corresponding r.m.s. values appear in the individual captions of figure 7). Going step by step through the critical regime the following phenomena can be observed: as mentioned before, the maximum $F_x(Re = 2.8\times10^5)$ in figure 6(c') marks the onset of broadband low-frequency fluctuations, which are called critical fluctuations, corresponding to the terminology used for phase transitions. In general, the occurrence of critical fluctuations indicates that a state of a physical system becomes unstable. The shaded part of the spectra in figure 7 represents the critical fluctuations. Continuous development of the spectra $\Phi_{\mathrm{L}}(f)$ up to the critical point immediately before transition A (figure 7b) is as follows: to the same extent as the peak becomes smaller and its width increases, the broadband low-frequency part of the spectrum increases (figure 7a, b). Immediately before transition A in the asymmetric bistable state, the spectrum (figures 7b, g) is characterized by two peaks, which, according to their Strouhal numbers, are probably related to the sub- and supercritical states. Furthermore, the high intensity of the critical fluctuations indicate that the flow is unstable to a high degree. In order to emphasize this

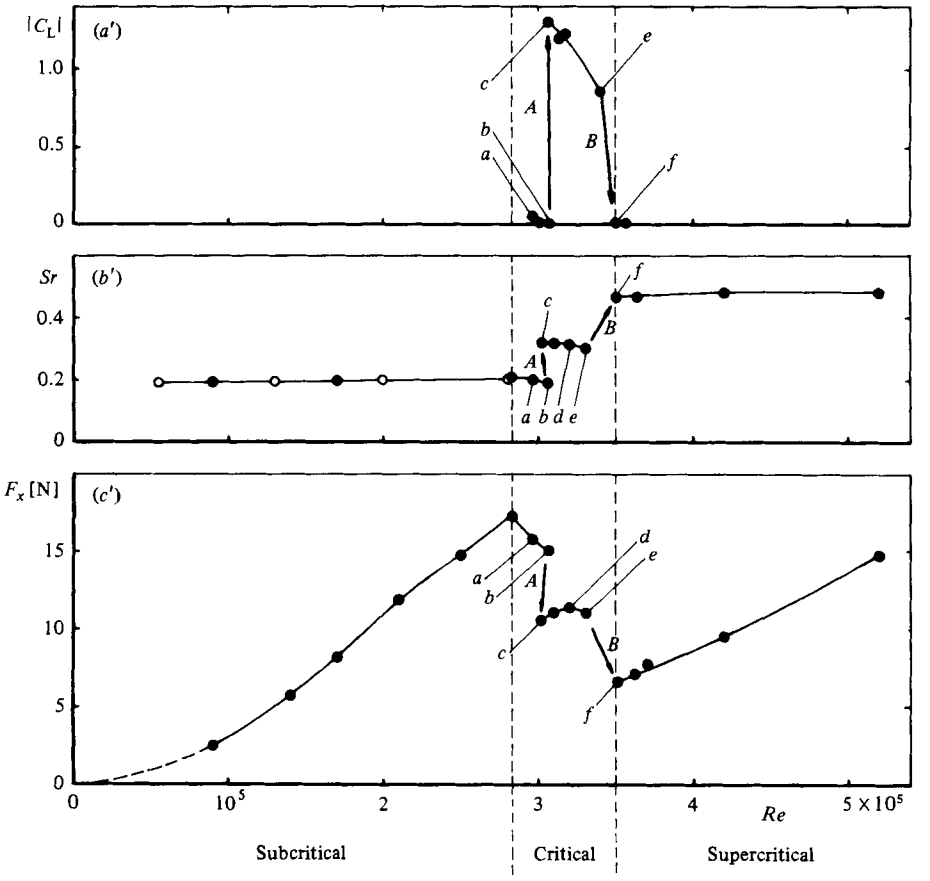

FIGURE 6. Fine structure in the critical range (the lower-case letters denote the individual stages of the flow state); ●, $p = 6$ bar; ○, $p = 2$ bar. (a') Absolute value of the steady lift coefficient $|C_L|$. (b') Strouhal number $Sr = fD/u_\infty$. (c') Drag force F_x.

important phenomenon of the occurrence of two peaks, a second spectrum of a different run is presented (figure 7*g*) where the two peaks are more pronounced. At this first critical point the state of the flow is probably jumping randomly in time and is randomly distributed along the axis of the cylinder from the sub- to the supercritical state, which is indicated by the two small peaks. It is conceivable that the process of jumping between the two states causes the wideband low-frequency fluctuations, the critical fluctuations. At this point of high instability of the flow it is sufficient in the experiment to wait until a perturbation of the flow itself is great enough to provoke transition A in the asymmetric flow state. This new state of the flow after transition A is stable, as can be concluded from the disappearance of the critical fluctuations (figure 7*c*) and the occurrence of a rather narrow peak at $Sr = 0.3$. With increasing Reynolds number the peak becomes smaller and the critical fluctuations occur again (figures 7*d*, *e*). Immediately before transition B there is a similar situation as before transition A. The peak has nearly vanished and the flow is unstable to a high degree. After transition B, the critical fluctuations have vanished and the mean flow field is symmetric again.

In figure 8 the power spectra of the lift $\Phi_L(f)$ and drag fluctuations $\Phi_D(f)$ are plotted for the bistable asymmetric state (stage *c*). It is remarkable that in this case

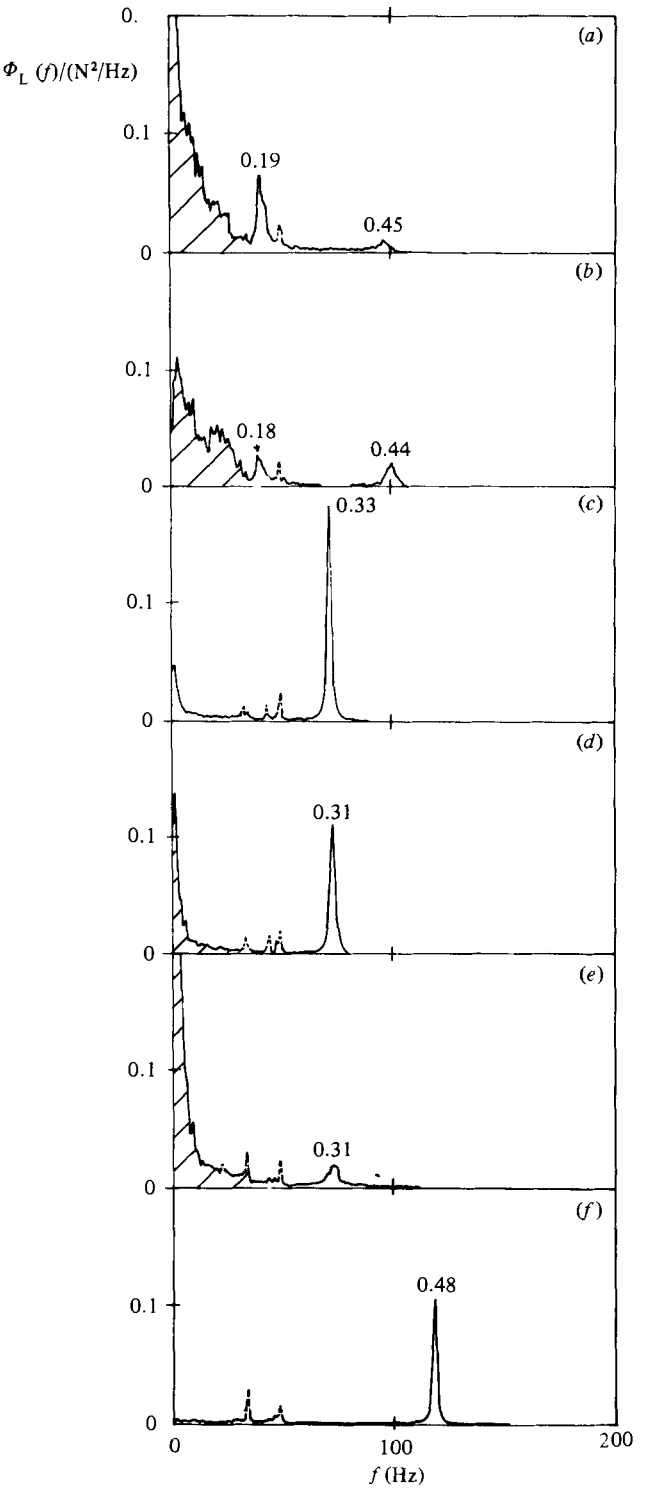

FIGURE 7. For caption see facing page.

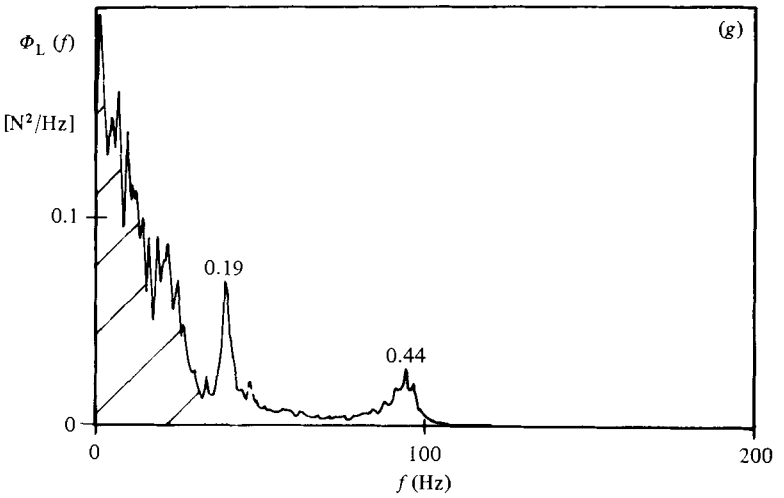

FIGURE 7. Power spectra of the lift fluctuations for the individual stages *a–f* in figure 6 (the Strouhal numbers of the peaks are included). (*a*) Typical spectrum near the critical *Re* with critical fluctuations (shaded), $(\overline{C_L^2})^{\frac{1}{2}} = 0.091$. (*b*) At the 1st critical *Re* immediately before transition *A*, $(\overline{C_L^2})^{\frac{1}{2}} = 0.062$. (*c*) Asymmetric bistable state immediately after transition *A*, $(\overline{C_L^2})^{\frac{1}{2}} = 0.044$. (*d*) The same state as in (*c*) with increased critical fluctuations as *Re* is slightly increased, $(\overline{C_L^2})^{\frac{1}{2}} = 0.045$. (*e*) At the 2nd critical *Re* immediately before transition *B*, $(\overline{C_L^2})^{\frac{1}{2}} = 0.067$. (*f*) Supercritical state immediately after transition *B* (the critical fluctuations have vanished), $(\overline{C_L^2})^{\frac{1}{2}} = 0.025$. (*g*) Stage as in (*b*), *Re* slightly lower.

the pronounced frequency of both components have the same value ($Sr = 0.33$). It is conceivable that, regarding the time-dependent behaviour of both force components, the dominating vortices are those which are shed from the side where the boundary-layer transition has not yet occurred. In the case of symmetric flow separation, for example for subcritical Reynolds numbers, the dominant frequency of the drag fluctuations has double the value of the dominant frequency of the lift fluctuations.

As is evident in figure 6, the speed in the wind tunnel is influenced by transitions *A* and *B* because of the fact that the changes of the drag of the cylinder are not small enough compared with the drag of the entire closed wind tunnel. After transition *A* the Reynolds number is slightly decreased and after transition *B* slightly increased. As the speed of the fan of the wind tunnel is kept constant by the controlling system, the drop of the drag of the cylinder (transition *B*) results in a small increase of the wind tunnel speed. After transition *A* the situation is more complicated. It is conceivable that the asymmetric flow leads to a slight impairment of the wind-tunnel performance, although the drag F_x on the cylinder is reduced. On the other hand, this undesired effect is a sensitive proof that transition *A* exhibits hysteresis. Without hysteresis the state of the flow would jump back to the state prior to transition *A* caused by the decreased wind-tunnel speed.

The hysteresis effect is demonstrated for example for the drag force F_x (figure 9). The transitions which occur with decreasing Reynolds number are denoted by a prime. It is obvious that, for decreasing Reynolds numbers $Re\downarrow$, the supercritical and bistable states can be maintained at lower Reynolds numbers than would be possible for increasing Reynolds numbers $Re\uparrow$.

In figure 10 the hysteresis effects are illustrated by means of the power spectra. The spectra recorded at transitions *A* and *B* (increasing Reynolds number *Re*) $Re\uparrow$ are identical with figures 7 (*f*, *e*, *b*): they are shown as dotted lines. In the same figures

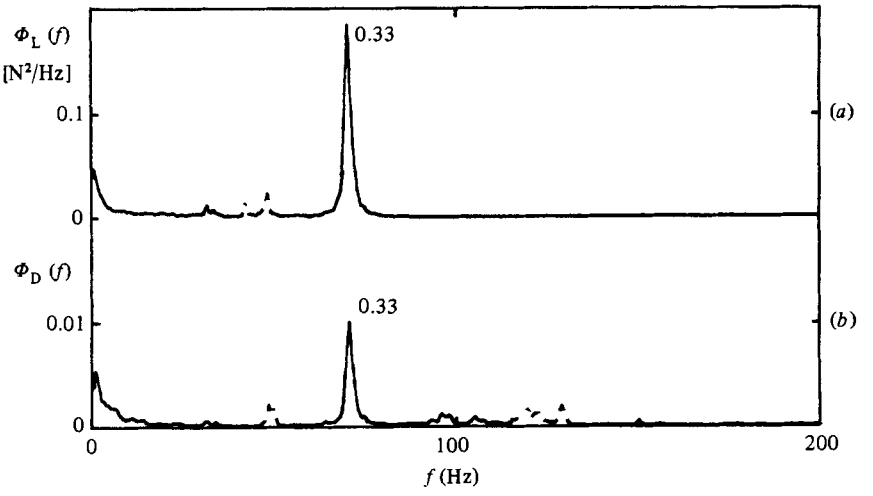

FIGURE 8. Power spectra of the lift (*a*) and drag (*b*) fluctuations in the asymmetric bistable state (stage *c* in figures 6 and 7).

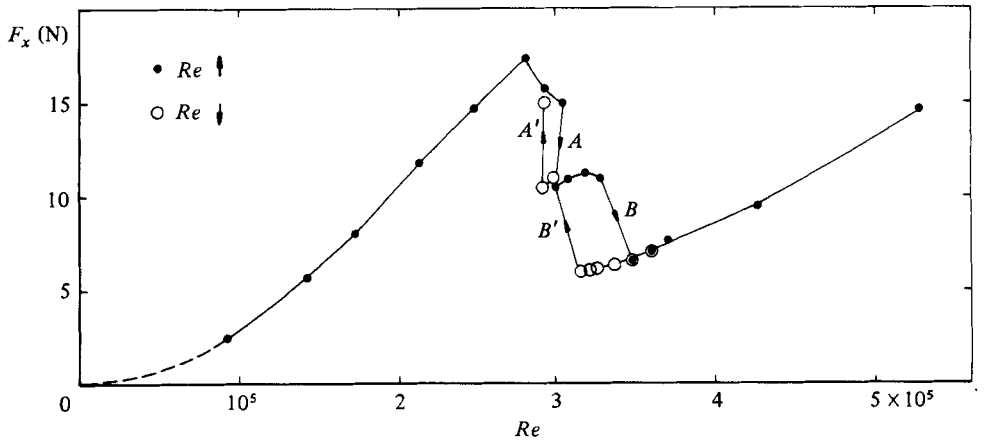

FIGURE 9. Hysteresis effects for transitions A and B (increasing $Re\uparrow$) and transition A' and B' (decreasing $Re\downarrow$); p = const = 6 bar.

the spectra are plotted, which were recorded at transitions A' and B' with decreasing Reynolds number $Re\downarrow$. In figure 10(*a*) the apparent shift of the peak to lower frequencies shows that the supercritical state can be maintained even at lower Reynolds numbers than would be possible for increasing Reynolds numbers $Re\uparrow$. The shift of the shedding frequency was caused by a corresponding decrease of the flow velocity u_∞.

For interpretation of figures 10(*b*, *c*) with respect to hysteresis, it is necessary to recall the sequence of the spectra in figure 7 and the related curve $F_x(Re)$ in figure 9. Both figures illustrate the individual successive stages of the flow in the critical regime. A direct comparison of the related spectra – i.e. immediately before (with $Re\uparrow$) and immediately after the transitions (with $Re\downarrow$) – shows that the latter spectra belong to a stage previous to the former ones.

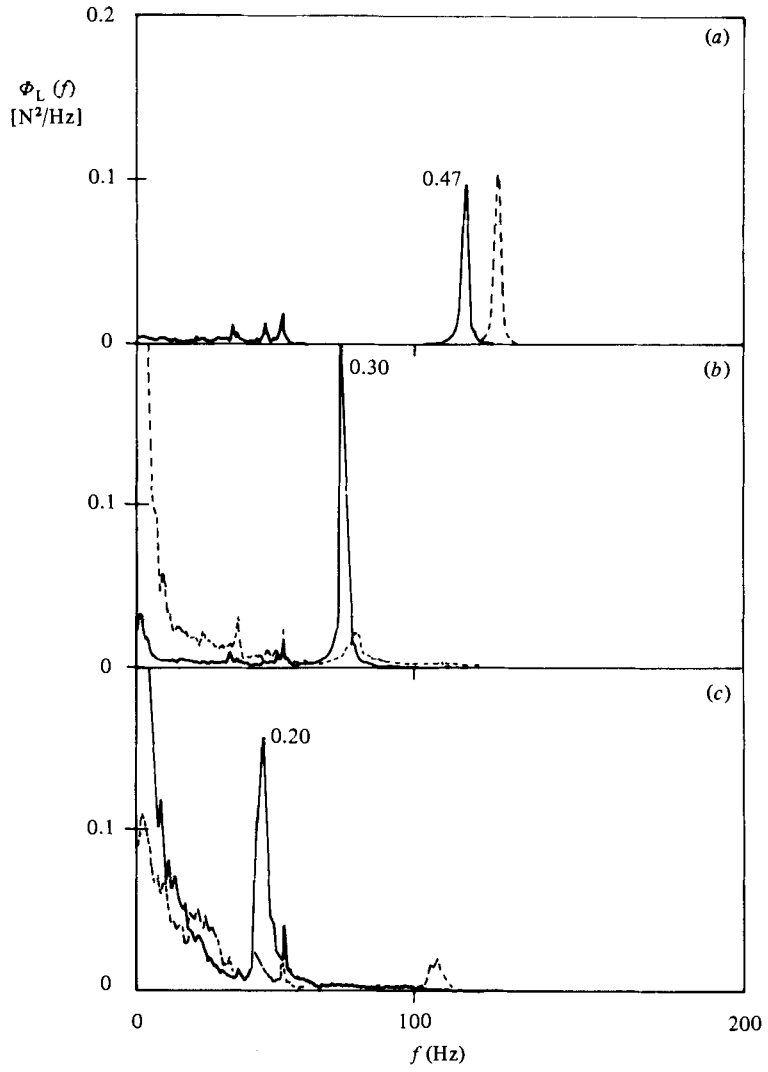

FIGURE 10. Power spectra immediately before and after the transitions (the corresponding Reynolds numbers are in figure 9). (*a*) ----, after transition *B* with *Re*↑; ——, before transition *B'* with *Re*↓. (*b*) ----, before transition *B* with *Re*↑; ——, after transition *B'* with *Re*↓. (*c*) ---- before transition *A* with *Re*↑; —— after transition *A'* with *Re*↓.

4. Discussion of the results

4.1. *Discussion of the phenomena occurring in the transitional ranges*

4.1.1. *The critical Reynolds-number range*

The explanation for the phenomena that occur lies in the behaviour of the boundary layer. The asymmetric flow and thus the steady lift in the critical range is caused by the fact that boundary-layer transition from laminar to turbulent has occurred on only one side of the cylinder. Thus a laminar separation bubble is formed as follows: the transition from laminar to turbulent flow occurs in the detached boundary layer just downstream from the separation point. After reattachment of the boundary layer on the back of the cylinder, the separation is turbulent. Thus the

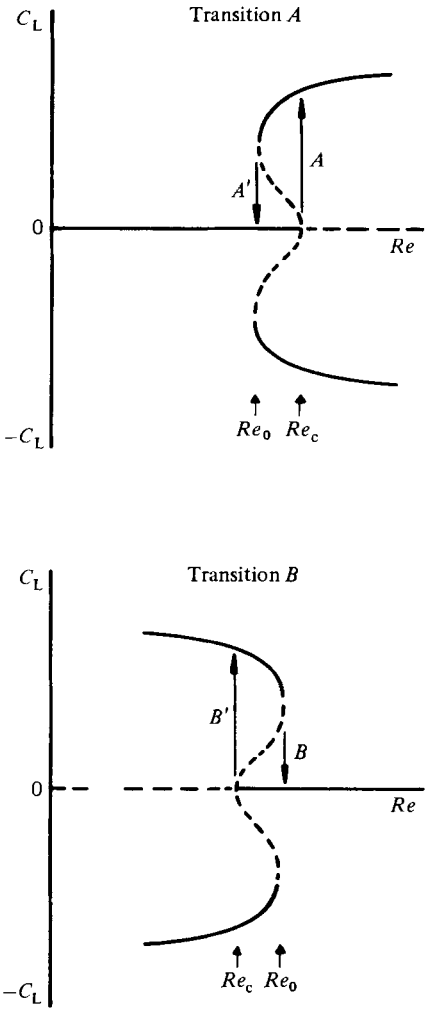

FIGURE 11. Schematic diagrams for subcritical bifurcations for transitions A and B (A' and B').

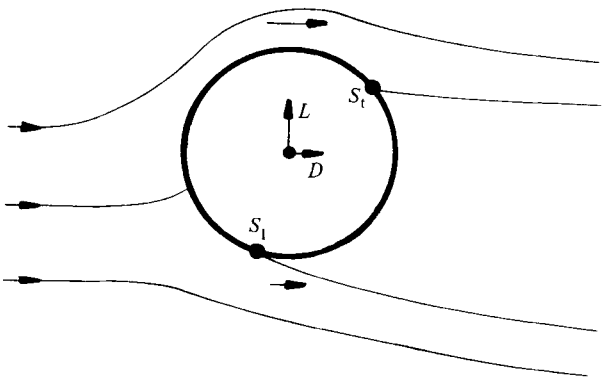

FIGURE 12. Simplified sketch of the asymmetric flow state in the critical regime (L = lift, D = drag, S_t = turbulent separation, S_l = laminar separation).

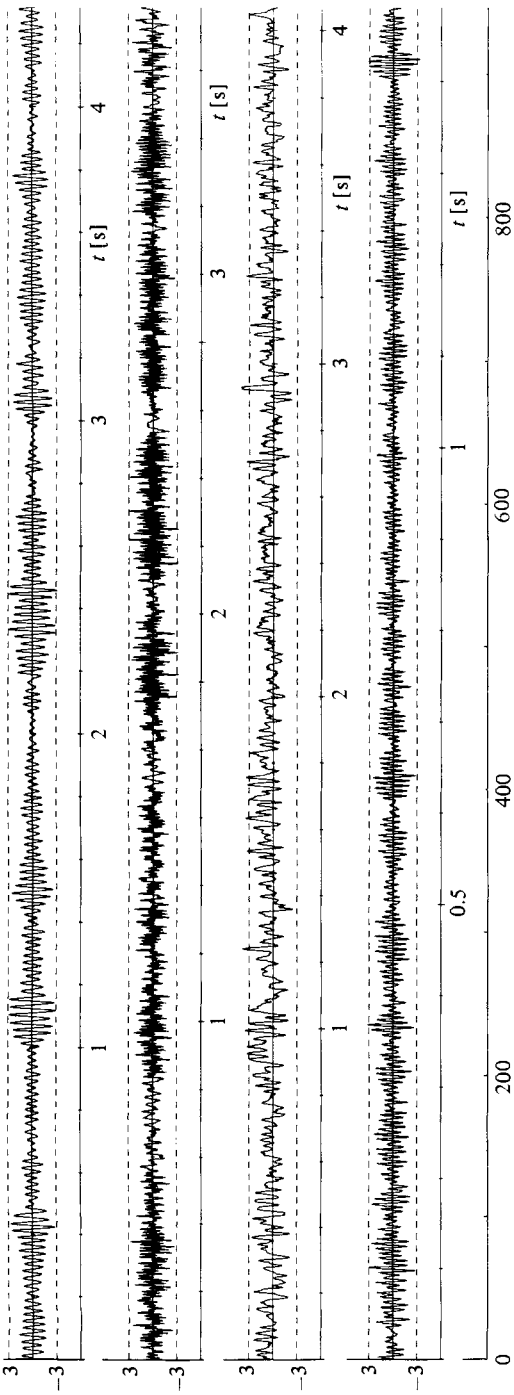

FIGURE 13. Time functions of the lift fluctuations for the individual Reynolds-number ranges, the amplitudes are normalized with the corresponding r.m.s. value – timescale Tu_∞/D is valid for all time functions. (*a*) Subcritical ($Re = 5.1 \times 10^4$). (*b*) Supercritical ($Re = 3.5 \times 10^5$). (*c*) Upper transition ($Re = 2.6 \times 10^6$). (*d*) Transcritical ($Re = 7.1 \times 10^6$).

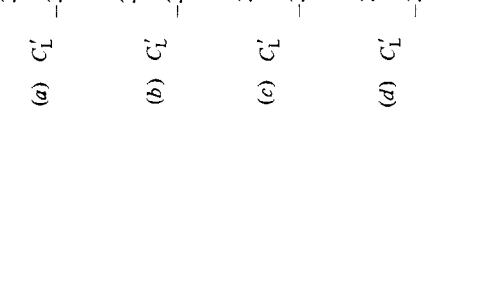

FIGURE 14. Time function of the drag and lift fluctuations taken at subcritical Reynolds number $Re = 2.4 \times 10^5$ (amplitudes are normalized with the corresponding r.m.s. value).

critical Reynolds number is reached if the distance between the separation point and the location of the transition in the detached boundary layer is small enough to allow reattachment. Transition B from asymmetric to symmetric flow is due to the formation of a second bubble on the other side of the cylinder.

The change from symmetric to asymmetric flow (transition A) is accompanied by generation of circulation around the cylinder, which causes the steady lift. In other words the process of changing states (transition A) generates the circulation. After the new state is established, the circulation remains constant (non-zero) in the mean. As a consequence of the circulation theorem, the rapid generation of the circulation must be accompanied by a starting vortex. The transition B can be explained in a similar manner.

Apart from this physical explanation for the steady lift force, there are many indications that the observed phenomena are caused by hydrodynamic instability, which can be treated in a general sense as phase transitions between two states of order. For both transitions A and B the following behaviour was observed, which is typical for subcritical bifurcations: critical fluctuations before the transitions (Figures 7*a*, *b*, *d*, *e*); the break of symmetry – which is at both transitions the sudden occurrence of the steady lift force (figure 6*a*′) – and finally the hysteresis effects (figures 9 and 10). In figure 11 the bifurcation diagrams for both transitions A and B are sketched separately, because of the fact that the state of the flow before transition A and after transition B is quite different, as can be concluded from the jumps of the Strouhal number and the drops of drag coefficient C_D. The parameter of stability is the Reynolds number at the abscissa, and the lift coefficient C_L was chosen as the order parameter, which characterizes the flow field. Unstable states of the flow are indicated by dotted and stable states by solid lines. Remembering the sequence of the spectra of the individual stages in the critical range (figure 7) the critical fluctuations occur when Re approaches Re_c. If the critical point Re_c is reached, the order parameter C_L takes a discontinuous jump on one of both possible stable branches – this is the break of symmetry ($C_L \neq 0$). Hysteresis is evident as transition A occurs at Re_c and transition A' at the somewhat lower Reynolds number Re_0. A corresponding explanation is valid for transition B in the supercritical state. Prior to transition B we are on one of the two stable branches; if the boundary of stability is reached the steady lift abruptly vanishes and the state of the flow is symmetric again. As was demonstrated by means of the drag force (figure 9) and the spectra (figure 10*a*) the supercritical state can be maintained for a slightly decreased Reynolds number because of the hysteresis until transition B' in the asymmetric state occurs at Re_c.

The following considerations are concerned with the process leading to the transitions: the boundary layer around the circular cylinder can be subdivided into two parts, which are separated in the mean by the stagnation line on the front of the cylinder. Although there is interaction between the two boundary layers, the transition on both sides at critical Reynolds numbers must not necessarily occur simultaneously. This supposition leads to the following speculations. Near the critical Reynolds number, the transition will be tripped by small perturbations, which is similar to a nucleation process typical for phase transitions in extended systems (Landauer 1978). Thus events in the microstructure of the flow can lead to changes in the macrostructure. At the critical point, the process leading to the transition in the detached boundary layer (free shear layer) will be initiated by perturbations or fluctuations, which are inherent in the boundary layer and the free stream. The occurrence of these perturbations is stochastic in space and time. The sign of the lift,

which characterizes the asymmetric flow, is dependent on the side where a perturbation sufficient to initiate the boundary-layer transition first occurs. The immediate formation of a one-sided bubble leads to steady circulation around the cylinder. This effect results in acceleration of the fluid on the side where the boundary-layer transition has occurred and in deceleration at the other side of the cylinder (figure 12). Deceleration of the fluid delays the transition in this detached boundary layer and hence the formation of the bubble. This coupled occurrence of the development of a bubble on one side with the deceleration of the fluid on the other side (i.e. decrease of the Reynolds number of this boundary layer) probably causes stabilizing and fixing of the asymmetric flow state. This effect is only possible if there is a very low probability for simultaneous occurrence of perturbations on both sides, which would be able to initiate simultaneous formation of both bubbles. The asymmetric state is stable for a small ΔRe until the boundary layer, which is not yet reattached, becomes unstable again while Re is increasing. If the second critical point is reached the second transition occurs, accompanied by the formation of the second bubble. We suppose that the width of the range ΔRe where the asymmetric flow state is stable and the width of the hysteresis range approaches zero is additional parameters of stability such as for example the turbulence intensity of the free stream or the surface roughness are increased.

4.1.2. *The transitional regime from super- to transcritical Reynolds numbers*

As already mentioned, it is established that in the supercritical state two stable laminar separation bubbles occur which are responsible for the low drag coefficient (see e.g. Roshko 1961; Tani 1964; Achenbach 1968; Bearman 1969). Roshko suggests in a general sense that disappearance of the separation bubbles characterizes the upper transition from super- to transcritical Reynolds numbers. Furthermore, it is possible that the stability and the dynamic behaviour of the separation bubbles are responsible for the occurring lifts (both signs were observed) and the pronounced maximum in the spectra at $Sr \approx 0.1$. The lift can be caused by a one-sided bubble and the pronounced maximum in the spectrum by a pulsating bubble.

It is conceivable that in this transitional range the flow around the cylinder passes through many successive phases of instability as in the critical regime until the transcritical regime is reached. These many individual transitions may be close together, making experimental investigation rather difficult. Finally it can be stated that the multivaluedness of the measured quantities for $10^6 \lesssim Re \lesssim 2 \times 10^6$ is caused by different states of the flow.

4.2. *Interpretation of time functions and probability densities*

Figures 13(*a–d*) show four time functions of the lift fluctuations typical for the individual Reynolds-number ranges. All amplitudes are normalized to their corresponding r.m.s. value and the dotted lines are equivalent to $\pm 3(\overline{C_L^2})^{\frac{1}{2}}$. The time axis was scaled with the inverse Strouhal number $1/Sr = Tu_\infty/D$; thus all time functions are directly comparable with respect to their characteristic time T. The time function in figure 13(*c*) taken at $Re = 2.6 \times 10^6$ (upper transition) is dominated by random fluctuations of the lift. This visual impression is confirmed by the corresponding probability density, which is nearly Gaussian. The time functions of the sub-, super- and transcritical ranges look like sine waves, which are randomly modulated in amplitude and frequency. Furthermore, the appropriate probability densities (figures 4 and 5) and their moments (table 1) deviate more or less from Gaussian, particularly in the case of subcritical Reynolds numbers. Under certain conditions, as mentioned

in §3.1.5, deviation from the Gaussian distribution allows conclusions concerning the physical nature of a process. The Central Limit Theorem can be reversed in a qualitative sense, such that deviation from the Gaussian distribution is an indication for cooperative behaviour (Haken 1982). Forces acting on the cylinder in crossflow are the result of a summation of many individual contributions (forces are integral values). In the case of statistical independence of the individual contributions, the summed value (the total force) obeys the Gaussian distribution provided that the number of contributions n is high ($n \to \infty$). This is a consequence of the Central Limit Theorem. On the other hand, the deviation from the Gaussian distribution indicates that the individual contributions are no longer independent but are correlated. Based on these considerations, the flow field around the cylinder in crossflow can be divided along its span into many subsystems. The instantaneous total force acting on the cylinder is then the result of the more or less cooperative behaviour of these individual subsystems, which differ slightly from each other in frequency and amplitude. Strong spanwise coherence leads to a wave train with peak values up to ± 3 r.m.s. in the subcritical state and about ± 4 r.m.s. in the super- and transcritical states. Small amplitudes of C'_{L} are the consequence of low coherence. In this context it is interesting to refer to figure 14, where for a subcritical Reynolds number the lift C'_{L} and the drag fluctuations C'_{D} are illustrated. It is evident that the modulation frequency of the amplitude of the lift fluctuations is strongly correlated with the very low-frequency fluctuations of the drag. In other words: if the amplitudes of the lift fluctuations are increasing, i.e. the coherence along the span of the cylinder increases, then the drag also increases and vice versa. The higher-frequency, which is obvious in drag fluctuations, has double the value of the shedding frequency; thus the spectrum contains a wide-band low-frequency part and a pronounced maximum at $Sr = 0.4$.

A consequence of these findings is that, up to a certain degree, a separation between the non-random and the random processes is possible. In the subcritical state, for example, the non-random process may be represented by a carrier frequency with $Sr = 0.2$, while the random processes are represented by the amplitude modulation of the carrier frequency and the wideband low-frequency fluctuations of the drag respectively.

The author would like to thank the Director of the Institute Prof. Dr H. Försching for initiating this investigation and for his interest. Further thanks go to Dr P. Bublitz for many discussions, suggestions and his continuous support. Gratitude is also expressed to the staff of the high-pressure wind tunnel, E. Melzer and his coworkers H. J. Bendig and H. Mittmann. The author is also indebted to Dr I. Rehberg for many discussions concerning the hydrodynamic-instability phenomena, and to R. Disselnkötter for his support in computer programming. This investigation was supported by the Deutsche Forschungsgemeinschaft (DFG).

REFERENCES

Achenbach, E. 1968 Distribution of local pressure and skin friction around a circular cylinder in cross-flow up to $Re = 5 \times 10^6$. *J. Fluid Mech.* **34**, 625.

Achenbach, E. & Heinecke, E. 1981 On vortex shedding from smooth and rough cylinders in the range of Reynolds numbers 6×10^3 to 5×10^6. *J. Fluid Mech.* **109**, 239.

Bearman, P. W. 1969 On vortex shedding from a circular cylinder in the critical Reynolds number regime. *J. Fluid Mech.* **37**, 577.

DRESCHER, H. 1956 Messung der auf querangeströmte Zylinder ausgeübten zeitlich veränderten Drücke. *Z. Flugwiss.* **4**, 17.

FÖRSCHING, H., MELZER, E. & SCHEWE, G. 1981 Ein neuer Windkanal für gebäudeaerodynamische und -aeroelastische Untersuchungen bei Reynoldszahlen bis 10^7. *DFVLR-AVA Rep.* IB 232-81 J 02, *Göttingen.*

HAKEN, H. 1982 *Synergetik – eine Einführung.* Springer. [English edition: *Synergetics – An Introduction.* Springer, 1978.]

JAMES, W. D., PARIS, S. W. & MALCOLM, G. N. 1980 Study of viscous crossflow effects on circular cylinder at high Reynolds numbers. *AIAA J.* **18**, 1066.

JONES, G. W., CINCOTTA, J. & WALKER, W. 1969 Aerodynamic forces on a stationary and oscillating circular cylinder at high Reynolds numbers. *NASA TR* R-300.

KAMIYA, N., SUZUKI, S. & NISHI, R. 1979 On the aerodynamic force acting on circular cylinder in the critical range of the Reynolds number. *AIAA Paper* 79-1475, *Williamsburg.*

KRAEMER, K. 1964 Druckverteilungsmessungen an Kreiszylindern mit Beachtung dreidimensionaler Randstörungen. *Mitt. MPI f. Strömungsforschung und AVA, Göttingen* no. 32.

LANDAUER, R. 1978 Stability in the dissipative steady state. *Phys. Today* (November), p. 23.

MORKOVIN, M. V. 1964 Flow around circular cylinder – a kaleidoscope of challenging fluid phenomena. In *Proc. Symp. on Fully Separated Flows* (ed. A. G. Hansen), p. 102. ASME.

ROSHKO, A. 1961 Experiments on the flow past a circular cylinder at very high Reynolds number. *J. Fluid Mech.* **10**, 345.

ROSHKO, A. 1970 On the aerodynamic drag of cylinders at high Reynolds numbers. *U.S.–Japan Research Seminar on Wind Loads on Structures, University of Hawaii, Oct.* 1970.

SCHEWE, G. 1982 A multicomponent balance consisting of piezoelectric force transducers for a high-pressure windtunnel. *Conf. Proc. Sensor & Systems* **82**, vol. 2, *Pasadena (USA)*, 18–20.5.82; and *Tech. Messen* **49**, 447 (German version).

TANI, J. 1964 Low-speed flows involving bubble separations *Prog. Aero. Sci.* **5**, 70.

WIESELSBERGER, C. 1923 Versuche über den Luftwiderstand gerundeter und kantiger Körper. *Ergebnisse Aerodyn. Versuchsanstalt Göttingen* (ed. L. Prandtl), II. Lieferung, p. 23.